# SPACE OBJECT MASS-SPECIFIC INERTIA MATRIX ESTIMATION FROM PHOTOMETRIC DATA

**Richard Linares***
***University at Buffalo, State University of New York, Amherst, NY, 14260-4400***
**Fred A. Leve†, Moriba K. Jah‡**
***Air Force Research Laboratory, Kirtland AFB, New Mexico, 87117***
**John L. Crassidis§**
***University at Buffalo, State University of New York, Amherst, NY, 14260-4400***

This works investigates the problem of estimating the scaled inertia parameters of a space object using photometric and astrometric data. The inertia matrix is parameterized in terms of the relative scaled inertias and the orientation of the principal components because the system is not completely observable. A Unscented Kalman Filter (UKF) is presented that processes the lightcurve (single band photometric) and angles (astrometric) data to estimate the orientation, rotational rates, position, and velocity of the space object (SO) along with the scaled inertia parameters.

## INTRODUCTION

Space Situational Awareness (SSA) is concerned with collecting and maintaining knowledge of all objects orbiting the Earth. A global network of radar and optical sensors collects the necessary data for coarse space-object-catalog development and maintenance. Some of these sensors are powerful ground-based telescopes that can resolve large SOs in Low Earth Orbit (LEO) such as the Hubble Space Telescope and the International Space Station to high detail. Unfortunately, most objects are too small and/or too distant to lend themselves to ground-based resolved imaging; such classes of objects are labeled as "unresolved objects." In particular, SOs in geosynchronous orbits, "micro" and "nano" satellites are too small to be resolved using ground-based optical telescopes and fall under the class of unresolved objects.

In addition, objects that are resolved may not acquire enough observations for accurate orbit predictions. Therefore, the change in orbit needs to be predicted accurately while measurements are unavailable. To predict the change in orbit accurately, while assuming the objects are rigid bodies, the knowledge of an objects mass, material properties, and inertia must be known. This is entirely due to the fact that non-conservative forces in space are position, attitude, and material property dependent (e.g., perturbations due to solar radiation pressure (SRP)), thus making the inference of the parameters, paramount.

*Graduate Student, Department of Mechanical & Aerospace Engineering. Email: linares2@buffalo.edu, Student Member AIAA.
†Research Engineer, Senior Member AIAA.
‡Senior Research Aerospace Engineer. Associate Fellow AIAA.
§Professor, Department of Mechanical & Aerospace Engineering. Email: johnc@buffalo.edu, Associate Fellow AIAA.

Much of the literature contains research that evaluates the exploitation of a spacecraft's onboard measurements to infer its own inertia.[1,2,3,4,5] Current research also evaluates the use of 3D imaging sensors to infer spacecraft mass properties from range and optical measurements.[6] To the best of the authors' knowledge, no literature exists that has evaluated the use of lightcurve data collected from ground based telescopes, to infer state, material, and mass properties of SOs at GEO simultaneously.

Even though the amount of light collected from many objects at GEO is small, optical observations may still be gathered to support orbit determination and space situational awareness (SSA) efforts. These observations cannot directly resolve the shape of the SO; however, by analyzing the time history of the measured brightness (i.e., lightcurves), one can infer physical properties. Such properties include the object's physical parameters such as surface characteristics, shape, and attitude dynamics. Past work has shown that SO shape and size information can be extracted from these data.[7]

This work examines the exploitation of the inferred angular velocity and attitude profile of a SO from lightcurve data to recover the scaled inertia matrix. The moments of inertia and mass distribution are tightly coupled with the rotational dynamics of an object, even though the observability of these quantities from attitude profiles may be low for particular angular velocities. Unless the attitude and material properties of the SO are known, one may only be able to observe the scaled inertia matrix (i.e., function of inertia ratios) rather than the full inertia matrix. In this work an estimation strategy is developed to quantify the scaled inertia matrix while making use of inertia matrix properties such as positive definiteness and symmetry. The observability of these quantities is examined using analytical formalisms and information-theoretic concepts such as mutual information and degenerate cases are identified. Supporting numerical simulations are provided for different SO angular velocity and attitude profiles to highlight the performance of the approach and observability issues.

**Rotational and Translational Models**

The two-body equations of motion with SRP accelerations are given by

$$\ddot{\mathbf{r}}^I = -\frac{\mu}{r^3}\mathbf{r}^I + \mathbf{a}^I_{\text{srp}}, \tag{1}$$

where $\mu$ is the gravitational parameter of the Earth, $r = \|\mathbf{r}^I\|$, and $\mathbf{a}^I_{\text{srp}}$ represents the acceleration perturbation due to SRP, which will be discussed in detail in the following section. The superscript $I$ denotes that the vectors are expressed in inertial coordinates

A number of parameterizations exist to specify attitude, including Euler angles, quaternions and Rodrigues parameters.[8] This paper uses the quaternion, which is based on the Euler angle/axis parametrization. The quaternion is defined as $\mathbf{q} \equiv [\boldsymbol{\varrho}^T \quad q_4]^T$ with $\boldsymbol{\varrho} = \hat{\mathbf{e}}\sin(\nu/2)$, and $q_4 = \cos(\nu/2)$, where $\hat{\mathbf{e}}$ and $\nu$ are the Euler axis of rotation and rotation angle, respectively. The quaternion must satisfy a unit norm constraint, $\mathbf{q}^T\mathbf{q} = 1$. In terms of the quaternion, the attitude matrix is given by

$$A(\mathbf{q}) = \Xi^T(\mathbf{q})\Psi(\mathbf{q}), \tag{2}$$

where

$$\Xi(\mathbf{q}) \equiv \begin{bmatrix} q_4 I_{3\times 3} + [\boldsymbol{\varrho}\times] \\ -\boldsymbol{\varrho}^T \end{bmatrix}, \tag{3a}$$

$$\Psi(\mathbf{q}) \equiv \begin{bmatrix} q_4 I_{3\times 3} - [\boldsymbol{\varrho}\times] \\ -\boldsymbol{\varrho}^T \end{bmatrix}, \tag{3b}$$

with

$$[\mathbf{a}\times] \equiv \begin{bmatrix} 0 & -a_3 & a_2 \\ a_3 & 0 & -a_1 \\ -a_2 & a_1 & 0 \end{bmatrix} \tag{4}$$

for any general $3 \times 1$ vector $\mathbf{a}$ defined such that the matrix form is equivalent to the vector cross product $[\mathbf{a}\times]\mathbf{b} = \mathbf{a} \times \mathbf{b}$.

The rotational dynamics are given by the coupled first-order differential equations:

$$\dot{\mathbf{q}}_I^B = \frac{1}{2}\Xi(\mathbf{q}_I^B)\boldsymbol{\omega}_{B/I}^B, \tag{5a}$$

$$\dot{\boldsymbol{\omega}}_{B/I}^B = J_{\text{SO}}^{-1}\left(\mathbf{T}_{\text{srp}}^B - \left[\boldsymbol{\omega}_{B/I}^B\times\right] J_{\text{SO}}\boldsymbol{\omega}_{B/I}^B\right), \tag{5b}$$

where $\boldsymbol{\omega}_{B/I}^B$ is the angular velocity of the SO with respect to the inertial frame, expressed in body coordinates (the notation superscript $B$ denotes that the vector is expressed in body coordinates), $J_{\text{SO}}$ is the inertia matrix of the SO and $\mathbf{T}_{\text{srp}}^B$ is the net torque acting on the SO due to SRP expressed in body coordinates.

For this work Eq. (5b) is rewritten in principal coordinates and the inertia matrix is expressed as $J_{\text{SO}} = C(\mathbf{q}_P^B)\, I\, C(\mathbf{q}_P^B)^T$, where $C(\mathbf{q}_P^B)$ is the orientation of the principal directions with respect to the body coordinates and $I = \text{diag}\left([I_1\, I_2\, I_3]\right)$ are the principal components. Then in principal coordinates Eq. (5b) becomes

$$\dot{\boldsymbol{\omega}}_{B/I}^P = \begin{bmatrix} \left(\frac{I_2-I_3}{I_1}\right)\omega_2\omega_3 \\ \left(\frac{I_3-I_1}{I_2}\right)\omega_3\omega_1 \\ \left(\frac{I_1-I_2}{I_3}\right)\omega_2\omega_1 \end{bmatrix}. \tag{6}$$

The inertia is inferred by estimation of the relative inertia ratios, then by defining

$$\boldsymbol{\mathcal{I}} \equiv \left[\left(\frac{I_2-I_3}{I_1}\right)\ \left(\frac{I_3-I_1}{I_2}\right)\ \left(\frac{I_1-I_2}{I_3}\right)\right]^T,$$

we can rewrite Eq. (6) as

$$\dot{\boldsymbol{\omega}}_{B/I}^P = \begin{bmatrix} p_1\omega_2\omega_3 \\ p_2\omega_3\omega_1 \\ p_3\omega_2\omega_1 \end{bmatrix}. \tag{7}$$

The quaternion kinematics can be written in terms of $\boldsymbol{\omega}_{P/I}^P$ by noting that $\boldsymbol{\omega}_{B/I}^B = \boldsymbol{\omega}_{B/P}^B + A(\mathbf{q}_P^B)\boldsymbol{\omega}_{P/I}^P$. Since the principal directions are fixed with respect to the body frame then $\boldsymbol{\omega}_{B/P}^B = \mathbf{0}$ and the quaternion kinematics is given by

$$\dot{\mathbf{q}}_I^B = \frac{1}{2}\Xi(\mathbf{q}_I^B)A(\mathbf{q}_P^B)\boldsymbol{\omega}_{P/I}^P. \tag{8}$$

The state that will be inferred in this work is given by

$$\mathbf{x} = [\mathbf{q}_I^{B^T}\ \mathbf{q}_P^{B^T}\ \boldsymbol{\omega}_{B/I}^{B^T}\ \mathbf{r}^{I^T}\ \mathbf{v}^{I^T}\ \boldsymbol{\mathcal{I}}]^T.$$

where $\mathbf{v}^I = \dot{\mathbf{r}}^I$. The following section will discuss the shape model and SRP model used in this work.

$$\boldsymbol{\omega}_{B/I}^B = A(\mathbf{q}_P^B)(\boldsymbol{\omega}_{B/P}^P + \boldsymbol{\omega}_{P/I}^P)$$

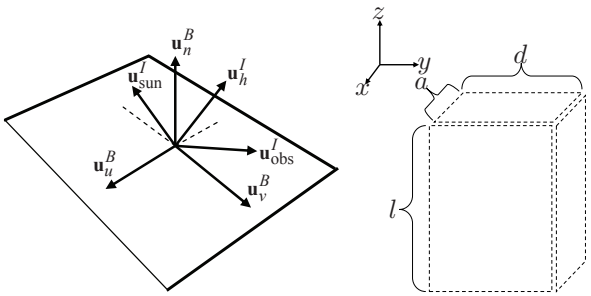


(a) Geometry of Reflection (b) Cuboid Shape Model

**Figure 1. Space Object Shape Model**

## SHAPE MODEL DEFINITION

The shape model considered in this work consists of a finite number a flat facets, where each facet has a set of basis vectors associated with it. These basis vectors are defined in Figure 1(a) and consist of three unit vectors $\mathbf{u}_n^B$, $\mathbf{u}_u^B$, and $\mathbf{u}_v^B$. The unit vector $\mathbf{u}_n^B$ points in the direction of the outward normal to the facet. For convex surfaces this model become more accurate as the number of facets are increased. The vectors $\mathbf{u}_u^B$ and $\mathbf{u}_v^B$ are in the plane of the facet. The SOs are assumed to be rigid bodies and therefore the unit vectors $\mathbf{u}_n^B$, $\mathbf{u}_u^B$ and $\mathbf{u}_v^B$ do not change since they are expressed in the body frame.

The lightcurve and the SRP models discussed in the next sections require that these vectors be expressed in inertial coordinates and since the SO body is rotating, these vectors will change with respect to the inertial frame. The body vectors can be rotated to the inertial frame by the standard attitude mapping given by:

$$\mathbf{u}_i^B = A(\mathbf{q}_I^B)\mathbf{u}_k^I, \quad k = u,\, v,\, n \tag{9}$$

where $A(\mathbf{q}_I^B)$ is the attitude matrix mapping the inertial frame to the body frame using the quaternion parameterization. Furthermore, the unit vector $\mathbf{u}_{\text{sun}}^I$ points from the SO to the Sun direction, and the unit vector $\mathbf{u}_{\text{obs}}^I$ points from the SO to the observer. The vector $\mathbf{u}_h^I$ is the normalized half vector between $\mathbf{u}_{\text{sun}}^I$ and $\mathbf{u}_{\text{obs}}^I$. This vector is also known as the Sun-SO-Observer bisector. Each facet has an area $\mathcal{A}(i)$ associated with it. Once the number of facets has been defined and their basis vectors are known, the areas $\mathcal{A}(i)$ define the size and shape of the SO. To determine the SRP forces and lightcurve characteristics, the surface properties must be defined for each facet.

For the development of the measured lightcurve data, faceted SO shape models are used. The rectangular model is described by three parameters, $l$, $a$, and $d$, which are the length, width, and height, respectively.

### Solar Radiation Pressure Model

For higher altitude objects ($\geq$ 1,000 km), SRP represents the primary non-conservative perturbation acting on SOs. Because SRP is dependent upon the SOs position and orientation, its effect couples the position and attitude dynamics.

For a SO comprised of a collection of $N$ flat facets as defined in Figure 1(a), the acceleration

perturbation due to SRP is given by[9,10]

$$\mathbf{a}^I_{\text{srp}} = \sum_{i=1}^{N} \mathbf{a}^I_{\text{srp}}(i), \tag{10a}$$

$$\mathbf{a}^I_{\text{srp}}(i) = \frac{-S_F \mathcal{A}(i) \cos^2(\theta(i))\, G[\cos(\theta(i))]}{m_{\text{SO}}\, c\, d^2} \mathbf{u}^I_{\text{srp}}(i), \tag{10b}$$

$$\mathbf{u}^I_{\text{srp}}(i) = 2\left[\frac{R_{\text{diff}}(i)}{3} + \frac{R_{\text{abs}}(i)\epsilon(i)}{3} + R_{\text{spec}}(i)\cos(\theta(i))\right]\mathbf{u}^I_n(i) + [1 - R_{\text{spec}}(i)]\mathbf{u}^I_{\text{sun}}, \tag{10c}$$

where $S_F = 1,367$ W/m$^2$ is referred to the solar constant and is a measure of the flux density of electromagnetic radiation incident on a sphere of radius 1 AU centered at the Sun, $c = 299,792,458$ m/s is the speed of light in a vacuum, $d$ is the distance between the SO and the Sun expressed in AU, $m_{\text{SO}}$ is the mass of the SO, $\epsilon(i)$, $\mathcal{A}(i)$ and $\mathbf{u}^I_n(i)$ are the emissivity, total area and normal vector for the $i^{\text{th}}$ facet and $R_{\text{spec}}(i)$, $R_{\text{diff}}(i)$ and $R_{\text{abs}}(i)$ are the spectral reflectance, diffuse reflectance and absorption coefficients which are assumed constant over the entire plate. Under the assumption that no energy is transmitted through the SO allows one to write

$$R_{\text{spec}}(i) + R_{\text{diff}}(i) + R_{\text{abs}}(i) = 1. \tag{11}$$

In addition, $\cos(\theta(i)) \equiv \left(\mathbf{u}^I_n(i)\right)^T \mathbf{u}^I_{\text{sun}}$ is the cosine of the inclination of the $i^{\text{th}}$ facet towards the Sun. The function $G[a] \equiv \max[0, \text{sign}(a)]$ will be zero when a side is shaded from the Sun (i.e. $\cos(\theta(i)) \leq 0$) and one when the facet is illuminated.

Equation (10b) can also be used in determining the torque on the SO due to SRP. Because the spectral, diffuse and absorption coefficients are constant over the entire facet, the contribution of SRP over the entire facet can be assumed to be a single force acting on the centroid of the facet. The total torque is then given by

$$T^B_{\text{srp}} = m_{\text{SO}} \sum_{i=1}^{N} \left[\boldsymbol{\ell}^B(i)\times\right]\left(A(\mathbf{q}^B_I)\mathbf{a}^I_{\text{srp}}(i)\right), \tag{12}$$

where $\boldsymbol{\ell}^B(i)$ is the position vector from the center of mass of the SO to the centroid of $i^{\text{th}}$ facet.

**Observation Model**

Consider observations made by a optical site which measures azimuth and elevation to a SO. The terminology associated measurement is defined where $\mathbf{d}^I$ is the position vector from the observer to the SO, $\mathbf{r}^I$ is the position of the SO in inertial coordinates, $\mathbf{R}^I$ is the radius vector locating the observer, $\alpha$ and $\delta$ are the right ascension and declination of the SO, respectively, $\theta$ is the sidereal time of the observer, $\lambda$ is the latitude of the observer, and $\phi$ is the East longitude from the observer to the SO. The fundamental observation is given by

$$\mathbf{d}^I = \mathbf{r}^I - \mathbf{R}^I. \tag{13}$$

In non-rotating equatorial (inertial) components the vector $\mathbf{d}^I$ is given by

$$\mathbf{d}^I = \begin{bmatrix} x - ||\mathbf{R}^I|| \cos(\theta)\cos(\lambda) \\ y - ||\mathbf{R}^I|| \sin(\theta)\cos(\lambda) \\ z - ||\mathbf{R}^I|| \sin(\lambda) \end{bmatrix}. \tag{14}$$

The conversion of $\mathbf{d}^I$ from the inertial to the observer coordinate system (Up-East-North) is given by

$$\begin{bmatrix} \rho_u \\ \rho_e \\ \rho_n \end{bmatrix} = \begin{bmatrix} \cos(\lambda) & 0 & \sin(\lambda) \\ 0 & 1 & 0 \\ -\sin(\lambda) & 0 & \cos(\lambda) \end{bmatrix} \times \begin{bmatrix} \cos(\theta) & \sin(\theta) & 0 \\ -\sin(\theta) & \cos(\theta) & 0 \\ 0 & 0 & 1 \end{bmatrix} \mathbf{d}^I. \tag{15}$$

The angle observations consist of the azimuth, az, and elevation, el. The observation equations are given by

$$\text{az} = \tan^{-1}\left(\frac{\rho_e}{\rho_n}\right), \tag{16a}$$

$$\text{el} = \sin^{-1}\left(\frac{\rho_u}{\|\mathbf{d}^I\|}\right). \tag{16b}$$

In addition to the azimuth and elevation, the optical site also records the magnitude of the brightness of the SO. The brightness of an object in space can be modeled using a Phong light diffusion model.[11] This model is based on the bidirectional reflectance distribution function (BRDF) which models light distribution scattered from the surface due to the incident light. The BRDF at any point on the surface is a function of two directions, the direction from which the light source originates, and the direction from which the scattered light leaves the observed surface. The model in Ref. [11] decomposes the BRDF into a specular component and a diffuse component. The two terms sum to give the total BRDF

$$\rho_{\text{total}}(i) = \rho_{\text{spec}}(i) + \rho_{\text{diff}}(i). \tag{17}$$

The diffuse component of Eq. (17), $\rho_{\text{diff}}(i)$ represents light that is scattered equally in all directions (Lambertian). The specular component of Eq. (17), $\rho_{\text{spec}}(i)$ represents light that is concentrated about some direction (mirror-like). Reference [11] develops a model for continuous arbitrary surfaces but simplifies for flat surfaces which is employed in this work. Therefore, the total observed brightness of an object becomes the sum of the contribution from each facet.

Under the flat facet assumption the specular term of the BRDF becomes[11]

$$\rho_{\text{spec}}(i) = \frac{\sqrt{(n_u+1)(n_v+1)}}{8\pi} \frac{\left(\mathbf{u}_n^I(i)\cdot\mathbf{u}_h^I\right)^{n_u(\mathbf{u}_h^I\cdot\mathbf{u}_u^I(i))^2+n_v(1-(\mathbf{u}_h^I\cdot\mathbf{u}_v^I(i))^2)}}{\mathbf{u}_n^I(i)\cdot\mathbf{u}_{\text{sun}}^I + \mathbf{u}_n^I(i)\cdot\mathbf{u}_{\text{obs}}^I - (\mathbf{u}_n^I(i)\cdot\mathbf{u}_{\text{sun}}^I)(\mathbf{u}_n^I(i)\cdot\mathbf{u}_{\text{obs}}^I)} F_{\text{reflect}}(i), \tag{18a}$$

where the Fresnel reflectance is given by

$$F_{\text{reflect}}(i) = R_{\text{spec}}(i) + \left(1 - R_{\text{spec}}(i)\right)\left(1 - \mathbf{u}_{\text{sun}}^I \cdot \mathbf{u}_h^I(i)\right)^5. \tag{19}$$

The parameters $n_u$ and $n_v$ of the Phong model dictate the direction (locally horizontal or vertical) distribution of the specular terms. The terms in Eq. (18) are functions of the reflection geometry which is described in Figure 1(a). The diffuse term of the BRDF for a single facet is

$$\rho_{\text{diff}}(i) = \left(\frac{28R_{\text{diff}}(i)}{23\pi}\right)(1 - R_{\text{spec}}(i))\left[1 - \left(1 - \frac{\mathbf{u}_n^I(i)\cdot\mathbf{u}_{\text{sun}}^I}{2}\right)^5\right]\left[1 - \left(1 - \frac{\mathbf{u}_n^I(i)\cdot\mathbf{u}_{\text{obs}}^I}{2}\right)^5\right]. \tag{20}$$

The apparent magnitude of a SO is the result of sunlight reflecting off of its surfaces along the line-of-sight to an observer. First, the fraction of visible sunlight that strikes an object (and not absorbed) is computed by

$$F_{\text{sun}}(i) = C_{\text{sun,vis}}\, \rho_{\text{total}}(i) \left(\mathbf{u}_n^I(i) \cdot \mathbf{u}_{\text{sun}}^I\right), \tag{21}$$

where $C_{\text{sun,vis}} = 455\ \text{W/m}^2$ is the power per square meter impinging on a given object due to visible light striking the surface. If either the angle between the surface normal and the observer's direction or the angle between the surface normal and Sun direction is greater than $\pi/2$, then there is no light reflected toward the observer. If this is the case, then the fraction of visible light is set to $F_{\text{sun}}(i) = 0$. Next, the fraction of sunlight that strikes an object that is reflected must be computed:

$$F_{\text{obs}} = \frac{F_{\text{sun}}(i)\mathcal{A}(i) \left(\mathbf{u}_n^I(i) \cdot \mathbf{u}_{\text{obs}}^I\right)}{\|\mathbf{d}^I\|^2}. \tag{22}$$

The reflected light is now used to compute the apparent brightness magnitude, which is measured by an observer:

$$m_{\text{app}} = -26.7 - 2.5\log_{10}\left|\sum_{i=1}^{N} \frac{F_{\text{obs}}(i)}{C_{\text{sun,vis}}}\right|, \tag{23}$$

where $-26.7$ is the apparent magnitude of the sun.

## UNSCENTED KALMAN FILTER FORMULATION

The unscented Kalman filter (UKF) is chosen for state estimation because it has at least the accuracy of a second-order filter[12] without the requirement of computing Jacobians like the extended Kalman filter (EKF). The UKF structure is used for estimating rotational, translational, and parameter states based on fusing angles and lightcurve data along with their associated models, as discussed in previous sections. The attitude UKF described in Ref. [13] is used in the same manner as the one shown in Refs. [14] and [15].

Applying the UKF structure for attitude estimation has some challenges. For instance, although three parameter sets are attitude minimal representations, they inherently have singularities. On the other hand, the quaternion representation, which is a four parameter set with no singularity, has a nonlinear constraint which results in a singular covariance matrix, and the quaternion is not constituted by directly adding quaternions but through quaternion composition. This does not allow use of quaternions in a straightforward UKF implementation. This work uses the method in Ref. [13], which overcomes these challenges by utilizing generalized Rodrigues parameters (GRPs), a three parameter set, to define the local error and quaternions to define the global attitude. The representation of the attitude error as a GRP is useful for the propagation and update stages of the attitude covariance because the structure of the UKF can be used directly. Complete explanations of the quaternion and its mapping to GRPs are provided in Refs. [8] and [16].

In the UKF implementation described in Ref. [13], the covariance matrix is interpreted as the covariance of the error GRP because for small angle errors the error GRP is additive and the UKF structure can be used directly to compute sigma-points. The error GRP sigma points are converted to error quaternions and then to global quaternions for the propagation stage. To compute the propagated covariance, the global quaternions are converted to error quaternions and then back to error GRPs. The process is then as follows: error GRP $\rightarrow$ error quaternion, error quaternion $\rightarrow$ global quaternion, global quaternion $\rightarrow$ error quaternion, and finally error quaternion $\rightarrow$ error GRP.

**Model and Measurement Uncertainty**

A UKF is now summarized for estimating the state of a SO's position, velocity, orientation, rotation rate, principal inertia components, and principal orientation given by

$$\mathbf{x} = [\mathbf{q}_I^{B^T}\ \mathbf{q}_P^{B^T}\ \boldsymbol{\omega}_{B/I}^{B^T}\ \mathbf{r}^{I^T}\ \mathbf{v}^{I^T}\ \boldsymbol{\mathcal{I}}]^T.$$

The dynamic models from Eqs. (1) and (5) can be written in the general state equation which gives the deterministic part of the stochastic model:

$$\dot{\mathbf{x}} = \mathbf{f}\left(\mathbf{x}, t\right) + G\left(\mathbf{x}, t\right)\boldsymbol{\Gamma}(t), \tag{24}$$

where $\boldsymbol{\Gamma}(t)$ is a Gaussian white noise process term with correlation function $Q\delta(t_1 - t_2)$. The function $\mathbf{f}\left(\mathbf{x}, t\right)$ is a general nonlinear function. To solve the general nonlinear filtering problem, the UKF utilizes the unscented transformation to determine the mean and covariance propagation though the function $\mathbf{f}\left(\mathbf{x}, t\right)$. The dynamic function used in this work consists of rotational and translational dynamics given by the sigma points, which are propagated through the system dynamics:

$$\mathbf{f}\left([\boldsymbol{\chi}, \hat{\mathbf{q}}]\right) = \begin{bmatrix} \frac{1}{2}\Xi(\mathbf{q}_I^B)A(\mathbf{q}_P^B)\boldsymbol{\omega}_{P/I}^P \\ \begin{bmatrix} p_1\omega_2\omega_3 \\ p_2\omega_3\omega_1 \\ p_3\omega_2\omega_1 \end{bmatrix} \\ -\frac{\mu}{r^3}\hat{\mathbf{r}}^I + \hat{\mathbf{a}}_{\text{SRP}}^I \end{bmatrix}. \tag{25}$$

If the initial pdf, $p(\mathbf{x}_o)$, that describes the associated state uncertainty is given, the solution for the time evolution of $p(\mathbf{x}, t)$ constitutes the nonlinear filtering problem.

Given a system model with initial state and covariance values, the UKF propagates the state vector and the error-covariance matrix recursively. At discrete observation times, the UKF updates the state and covariance matrix conditioned on the information gained from the measurements. The prediction phase is important for overall filter performance. In general, the discrete measurement equation can be expressed for the filter as

$$\tilde{\mathbf{y}}_k = \mathbf{h}\left(\mathbf{x}_k, t_k\right) + \mathbf{v}_k, \tag{26}$$

where $\tilde{\mathbf{y}}_k$ is a measurement vector and $\mathbf{v}_k$ is the measurement noise, which is assumed to be a zero-mean Gaussian process with covariance $R_k$.

All random variables in the UKF are assumed to be Gaussian random variables and their distributions are approximated by deterministically selected sigma points. The sigma points are selected to be along the principal axis directions of the state error-covariance. Given an $L \times L$ error-covariance matrix $P_k$, the sigma points are constructed by

$$\boldsymbol{\sigma}_k \leftarrow 2L \text{ columns from } \pm\sqrt{(L+\lambda)P_k}, \tag{27a}$$

$$\boldsymbol{\chi}_k(0) = \boldsymbol{\mu}_k, \tag{27b}$$

$$\boldsymbol{\chi}_k(i) = \boldsymbol{\sigma}_k(i) + \boldsymbol{\mu}_k, \tag{27c}$$

where $\sqrt{M}$ is shorthand notation for a matrix $Z$ such that $M = Z\,Z^T$. Given that these points are selected to represent the distribution of the state vector, each sigma point is given a weight that

preserves the information contained in the initial distribution:

$$W_0^{\text{mean}} = \frac{\lambda}{L+\lambda}, \tag{28a}$$

$$W_0^{\text{cov}} = \frac{\lambda}{L+\lambda} + (1-\alpha^2+\beta), \tag{28b}$$

$$W_i^{\text{mean}} = W_i^{\text{cov}} = \frac{1}{2(L+\lambda)}, \quad i = 1,\, 2,\, \ldots,\, 2L, \tag{28c}$$

where $\lambda = \alpha^2(L+\kappa) - L$ is a composite scaling parameter.

The constant $\alpha$ controls the spread of the sigma point distribution and should be a small number, $0 < \alpha \leq 1$. The constant $\kappa = 3 - L$ provides an extra degree of freedom that is used to fine-tune the higher-order moments, and $\beta$ is used to incorporate prior knowledge of the distribution by weighting the mean sigma point in the covariance calculation.

The reduced state vector, with the error GRP states for the joint attitude, position, and inertia estimate problem are given by

$$\hat{\mathbf{x}}_k^{\boldsymbol{\delta}\mathbf{p}} = \left.\begin{bmatrix} \boldsymbol{\delta}\hat{\mathbf{p}}_I^B \\ \boldsymbol{\delta}\hat{\mathbf{p}}_P^B \\ \hat{\boldsymbol{\omega}}_{B/I}^B \\ \hat{\mathbf{r}}^I \\ \hat{\mathbf{v}}^I \\ \boldsymbol{\mathcal{I}} \end{bmatrix}\right|_{t_k}, \tag{29}$$

where $\boldsymbol{\delta}\hat{\mathbf{p}}$ are the error GRP states associated with the quaternion $\hat{\mathbf{q}}_I^B$ and $\hat{\cdot}$ is used to denote estimate. The initial estimate $\hat{\mathbf{x}}_0$ is the mean sigma point and is denoted $\boldsymbol{\chi}_0(0)$. The error GRP state of the initial estimate is set to zero, while the rest of the states are initialized by their respective initial estimates.

**Using Quaternions for UKF**

The error quaternion, denoted by $\boldsymbol{\delta}\mathbf{q}_k^-(i)$, associated with the $i^{\text{th}}$ error GRP sigma point is computed by[13]

$$\boldsymbol{\delta}\boldsymbol{\varrho}_k^-(i) = f^{-1}\left[a + \delta q_{4_k}^-(i)\right]\boldsymbol{\chi}_k^{\delta p}(i), \tag{30a}$$

$$\delta q_{4_k}^-(i) = \frac{-a||\boldsymbol{\chi}_k^{\delta p}(i)||^2 + f\sqrt{f^2 + (1-a^2)||\boldsymbol{\chi}_k^{\delta p}(i)||^2}}{f^2 + ||\boldsymbol{\chi}_k^{\delta p}(i)||^2}, \tag{30b}$$

$$\boldsymbol{\delta}\mathbf{q}_k^-(i) = \begin{bmatrix} \boldsymbol{\delta}\boldsymbol{\varrho}_k^-(i) \\ \delta q_{4_k}^-(i) \end{bmatrix}, \tag{30c}$$

where $a$ is a parameter from 0 to 1 and $f$ is a scale factor, which is often set to $f = 2(a+1)$. Here it is noted that the subscript $I$ and superscript $B$ in $\mathbf{q}_I^B$ and its estimates are omitted in this section for brevity. The representation of the attitude estimate perturbed by the $i^{\text{th}}$ error quaternion is computed using the quaternion composition:

$$\hat{\mathbf{q}}_k^-(i) = \boldsymbol{\delta}\mathbf{q}_k^-(i) \otimes \hat{\mathbf{q}}_k^-(0) \tag{31}$$

, where

$$\mathbf{q}' \otimes \mathbf{q} = \begin{bmatrix} \Psi(\mathbf{q}') & \mathbf{q}' \end{bmatrix}\mathbf{q}. \tag{32}$$

This forms the global quaternion. The error quaternions corresponding to each propagated quaternion sigma point are computed through the quaternion composition:

$$\boldsymbol{\delta}\mathbf{q}^{-}_{k+1}(i) = \hat{\mathbf{q}}^{-}_{k+1}(i) \otimes \left[\hat{\mathbf{q}}^{-}_{k+1}(0)\right]^{-1}, \tag{33}$$

where the notation for the inverse quaternion is defined as:

$$\mathbf{q}^{-1} \equiv \begin{bmatrix} -\boldsymbol{\varrho} \\ q_4 \end{bmatrix}. \tag{34}$$

Using the result of Eq. (33), the error GRP sigma points are computed as

$$\boldsymbol{\delta}\mathbf{p}^{-}_{k+1}(i) = f\frac{\boldsymbol{\delta}\hat{\boldsymbol{\varrho}}^{-}_{k+1}(i)}{a + \delta\hat{q}^{-}_{4_{k+1}}(i)}. \tag{35}$$

Angles data can be used to determine the unknown position and velocity of a SO. However, if the position is coupled with the attitude dynamics, then angles data can assist with attitude estimation as well. However if position is known accurately, then using only lightcurve data is sufficient to determine the orientation.

**Summary of UKF**

The UKF algorithm is described in Table 1. The process starts by first defining two initial state vectors, one that includes quaternion states and one that includes error GRP states. The error GRP states are initially set to zero. The initial covariance matrix is defined as the initial error covariance for the state vector that includes the GRP states, the translational, rotational and parametric states. The covariance matrix is then used to form the error GRP sigma points. The error GRP sigma points are converted to quaternion sigma points by creating error quaternions from each error GRP and then adding the error quaternion to the initial mean quaternion using quaternion multiplication.

Next the quaternion sigma points are propagated through the system dynamics using equation Eq. (25). The estimated acceleration and torque due to SRP are calculated with Eqs. (10) and (12), respectively. After propagating the sigma points, the error GRP states are computed with the propagated quaternion sigma points. The propagated mean sigma point quaternion, $\hat{\mathbf{q}}^{-}_{k+1}(0)$, is computed and stored, and error quaternions corresponding to each propagated quaternion sigma point are computed. The non-attitude sigma points are the propagated non-attitude states.

After setting the error GRP for the mean sigma point to zero, the propagated sigma points are recombined, and the propagated mean and covariance are calculated as a weighted sum of the sigma points, where $Q_{k+1}$ is the discrete-time process noise covariance. As previously discussed, measurements are available in the form of azimuth, elevation and apparent brightness magnitude, $\tilde{\mathbf{y}} \equiv [\tilde{m}_{\text{app}} \quad \tilde{\text{az}} \quad \tilde{\text{el}}]^T$. Estimated observations are computed for each sigma point using the observation models discussed previously. The mean estimated output are computed, and the output, innovations, and cross-correlation covariance are computed using the sigma points.

Finally, the Kalman gain is calculated from the sigma point and is used to update the estimated state vector that contains the error GRPs. The quaternion update is performed by converting the error GRP states of $\hat{\mathbf{x}}^{+}_{k}$ to a quaternion, $\boldsymbol{\delta}\hat{\mathbf{q}}^{+}_{k}$, via Eq. (30), and adding it to the estimated quaternion using quaternion multiplication.

**Table 1. UKF for Rotational, Translational, and Parameter States**

| |
|---|
| Initialize with<br>$\hat{\mathbf{x}}_o^{\boldsymbol{\delta}\mathbf{p}} = E\{\mathbf{x}_o^{\boldsymbol{\delta}\mathbf{p}}\} \quad \hat{\mathbf{x}}_o^{\mathbf{q}} = E\{\mathbf{x}_o\} \quad \mathbf{P}_o^{\boldsymbol{\delta}\mathbf{p}} = E\{\left(\mathbf{x}_o^{\boldsymbol{\delta}\mathbf{p}} - \hat{\mathbf{x}}_o^{\boldsymbol{\delta}\mathbf{p}}\right)\left(\mathbf{x}_o^{\boldsymbol{\delta}\mathbf{p}} - \hat{\mathbf{x}}_o^{\boldsymbol{\delta}\mathbf{p}}\right)^T\}$ |
| Calculate GRP Sigma Points<br>$\boldsymbol{\chi}_k^{\boldsymbol{\delta}\mathbf{p}} = \left[\hat{\mathbf{x}}_k^{\boldsymbol{\delta}\mathbf{p}} \quad \hat{\mathbf{x}}_k^{\boldsymbol{\delta}\mathbf{p}} + \gamma\sqrt{P_{k-1}} \quad \hat{\mathbf{x}}_k^{\boldsymbol{\delta}\mathbf{p}} - \gamma\sqrt{P_{k-1}}\right]$<br>Calculate Quaternion Sigma Points<br>$\boldsymbol{\chi}_k^{\mathbf{q}} = \left[\hat{\mathbf{x}}_k^{\mathbf{q}} \quad \hat{\mathbf{x}}_k^{\mathbf{q}} + \gamma\sqrt{P_{k-1}} \quad \hat{\mathbf{x}}_k^{\mathbf{q}} - \gamma\sqrt{P_{k-1}}\right]$ |
| Propagate Quaternion Sigma Points<br>$\boldsymbol{\chi}_k^{\mathbf{q}} = \mathbf{F}\left[\boldsymbol{\chi}_{k-1}^{\mathbf{q}}, t\right]$<br>Calculate GRP Sigma Points<br>$\boldsymbol{\chi}_k^{\boldsymbol{\delta}\mathbf{p}} = \left[\hat{\mathbf{x}}_k^{\boldsymbol{\delta}\mathbf{p}} \quad \hat{\mathbf{x}}_k^{\boldsymbol{\delta}\mathbf{p}} + \gamma\sqrt{P_{k-1}} \quad \hat{\mathbf{x}}_k^{\boldsymbol{\delta}\mathbf{p}} - \gamma\sqrt{P_{k-1}}\right]$ |
| Time update<br>$\hat{\mathbf{x}}_{k+1}^- = \sum_{i=0}^{2L} W_i^{\text{mean}}\, \boldsymbol{\chi}_{k+1}(i)$<br>$P_{k+1}^- = \sum_{i=0}^{2L} W_i^{\text{cov}}\left[\boldsymbol{\chi}_{k+1}(i) - \hat{\mathbf{x}}_{k+1}^-\right]\left[\boldsymbol{\chi}_{k+1}(i) - \hat{\mathbf{x}}_{k+1}^-\right]^T + Q_{k+1}$ |
| Measurement update<br>$\boldsymbol{\gamma}_k(i) = \mathbf{h}\left[\boldsymbol{\chi}_k(i), \hat{\mathbf{q}}_k^-\right]$<br><br>$\hat{\mathbf{y}}_k^- = \sum_{i=0}^{2L} W_i^{\text{mean}}\, \boldsymbol{\gamma}_k(i)$<br>$P_k^{yy} = \sum_{i=0}^{2L} W_i^{\text{cov}}\left[\boldsymbol{\gamma}_k(i) - \hat{\mathbf{y}}_k^-\right]\left[\boldsymbol{\gamma}_k(i) - \hat{\mathbf{y}}_k^-\right]^T$<br>$P_k^{vv} = P_k^{yy} + R_k$<br>$P_k^{xy} = \sum_{i=0}^{2L} W_i^{\text{cov}}\left[\boldsymbol{\chi}_k(i) - \hat{\mathbf{x}}_k^-\right]\left[\boldsymbol{\gamma}_k(i) - \hat{\mathbf{y}}_k^-\right]^T$<br>$K_k = P_k^{xy}(P_k^{vv})^{-1}$<br>$\hat{\mathbf{x}}_k^+ = \hat{\mathbf{x}}_k^- + K_k\left[\tilde{\mathbf{y}}_k - \hat{\mathbf{y}}_k\right]$<br>$P_k^+ = P_k^- - K_k P^{vv} K_k^T$ |
| Quaternion update<br>$\hat{\mathbf{q}}_k^+ = \boldsymbol{\delta}\hat{\mathbf{q}}_k^+ \otimes \hat{\mathbf{q}}_k^-(0)$<br>Set GRP to zero<br>$\boldsymbol{\delta}\mathbf{p} = [0 \quad 0 \quad 0]^T$ |

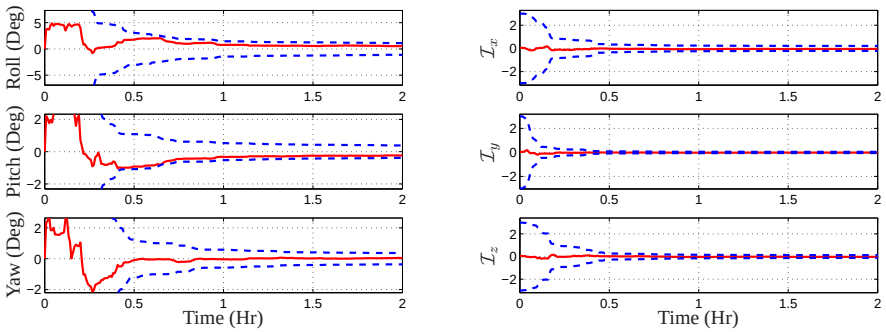


(a) Principal Orientation Estimation Error (b) Relative Inertia Estimation Error

**Figure 2. Spacecraft State Inertia Estimation Results**

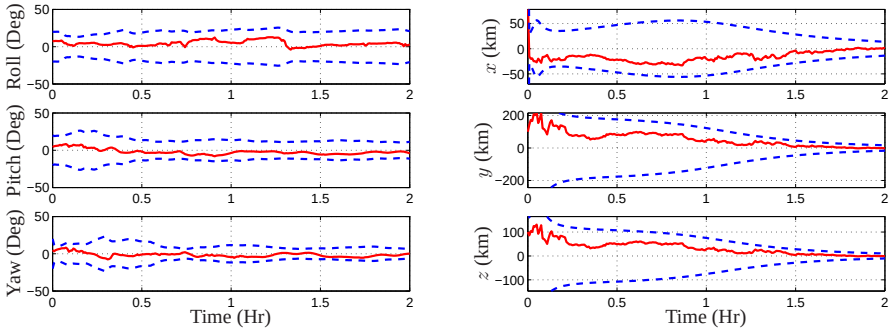


(a) Attitude Estimation Error (b) Position Estimation Error

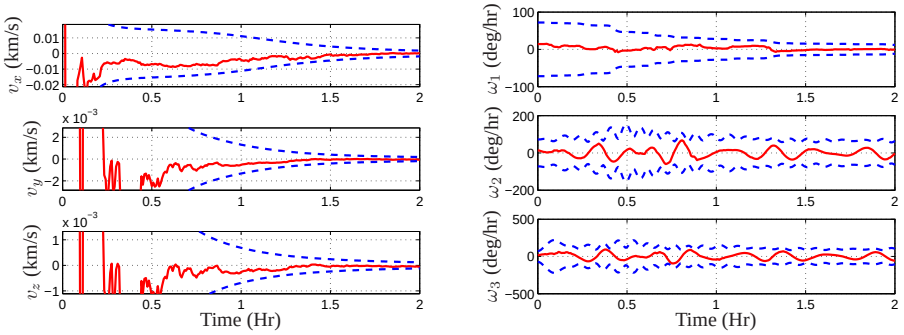


(c) Velocity Estimation Error (d) Angular Velocity Estimation Error

**Figure 3. Spacecraft State Estimation Results**

## SIMULATION RESULTS

A simulation is presented to determine the estimator's performance. An equatorial ground station is chosen as the site of the observer for the truth model. In addition, the scenario uses a shape model which contains six sides. The SO is simulated to orbit in a continuously sunlit near-geosynchronous regime. This is accomplished by inclining the orbit by $30$ degrees and choosing an appropriate time of the year, thereby avoiding the shadow cast by the Earth.

The initial inertial position and velocity are chosen as $\mathbf{r}^I = [-7.8931\times10^2 \;\; 3.6679\times10^4 \;\; 2.1184\times 10^4]^T$ km and $\mathbf{v}^I = [-3.0669 \;\; -4.9425\times10^{-2} \;\; -2.8545\times10^{-2}]^T$ km/s. The geographic position of the ground site is $0^\circ$ North, $172^\circ$ West with $0$ km altitude. The time epoch of the simulation is May $8$, $2007$ at 5:27.55. The initial true quaternion attitude mapping from the inertial frame to the body frame is chosen as $\mathbf{q}_I^B = [1/2 \;\; 0 \;\; 0 \;\; 1/2]^T$. A constant rotation rate, defined as the body rate with respect to the inertial frame, represented in body coordinates, is used and given by $\boldsymbol{\omega}_{B/I}^B = [0.00262 \;\; 0.002 \;\; 0]^T$ rad/s. A constant rotation rate, defined as the body rate with respect to the inertial frame, represented in body coordinates, is used and given by $\boldsymbol{\omega}_{B/I}^B = [0.00262 \;\; 0.002 \;\; 0.0002]^T$ rad/s. The shape parameters of the SO are given by $a = 8.9443$ m, $d = 8.9443$ m, and $l = 7.8262$ m. The true inertia parameters are by $\mathbf{q}_I^P = [0 \;\; 0 \;\; 0 \;\; 1]^T$, and $I = \text{diag}([1500 \;\; 1000 \;\; 100])$ kg$-$m$^2$ where $\boldsymbol{\mathcal{I}} = [0.60 \;\; -1.4 \;\; 5.0]^T$.

For all simulation scenarios, measurements are generated using zero-mean white-noise error processes with standard deviation of $0.5$ arc-seconds for azimuth and elevation. The initial errors for the states are $1$ km and $0.001$ km/s for the position and the velocity, respectively. The initial condition error-covariance values are set to $1^2$ km$^2$ and $0.001^2$ (km/s)$^2$ for the position and the velocity errors, respectively. The time interval between the measurements is set to $20$ seconds. Data are simulated for $1$ nights where observations of the SO are made over a $2$ hour period.

The estimation errors, along with their respective $3\sigma$ bounds calculated from the covariance for attitude, position, velocity, rotation rate, are shown in Figure 3. The attitude is estimated to within $10^\circ$ $3\sigma$ of uncertainty, and attitude rate is found to within $20$ deg/hr $3\sigma$ for the $x$-axis, $y$-axis, and for the $z$-axis. Position and velocity are estimated to within $10$ m and $0.0028$ m/s, respectively. The scaled principal inertia ratios are estimated to within $1$ percent $3\sigma$, and the principal orientation is estimated to $10^\circ$ $3\sigma$. Also, the roll axis principal orientation and the first scaled inertia parameter plot shows in Figure 2 that these parameters are not completely observable. This is due to the fact that the spin of SO does not excite the system to span these parameters. Although these parameters are weakly observable, the filter can still observe the remaining relative inertias. The kinematic states in Figures 2 and 3 show proper filter convergence behavior in that, the residual errors settle down and are bounded by their computed $3\sigma$ bounds.

## CONCLUSION

An UKF estimation scheme using lightcurve and angles data was used to estimate scaled inertias and the orientation of the principal directions of an SOalong with its associated rotational and translational states. This work uses an assumed shape model of six sides and estimated scaled inertia parameters for the SO. Using a UKF to employ brightness magnitude and angles data, the estimator was able to determine the scaled inertia parameters of an SO to within $1$ percent for the scaled inertia and $5$ degs for the orientation of the principal directions. Simulations were conducted to study estimate accuracy. Adequate performance was found for the estimator and the errors were well within the $3\sigma$ bounds.

## REFERENCES


[1] Yoon, H. and Tsiotras, P., "Adaptive Spacecraft Attitude Tracking Control with Actuator Uncertainties," *AIAA Guidance, Navigation, and Control Conference*, 2005s.

[2] Chaturvedi, N. A., Bernstein, D. S., Ahmed, J., Bacconi, F., and McClamroch, N. H., "Globally Convergent Adaptive Tracking of Angular Velocity and Inertia Identification for a 3-DOF Rigid Body," *IEEE Transactions on Control System Technology*, Vol. 14, No. 5, Sept. 2006.

[3] Ahmed, J., Coppola, V. T., and Bernstein, D. S., "Adaptive Asymptotic Tracking of Spacecraft Attitude Motion with Inertia Matrix Identification," *AIAA Journal of Guidance, Control, and Dynamics*, Vol. 21, No. 5, Sept-Oct 1998.

[4] Devon, D. A. and Fuentes, R. J., "Adaptive Attitude Control and Closed-Loop Power Tracking for and Integrated Power and Attitude Control System using Variable Speed Control Moment Gyroscopes," *AIAA Guidance, Navigation, and Control Conference*, 2005.

[5] Mackunis, W., Dupree, K., Fitz-Coy, N., and Dixon, W., "Adaptive Neural Network Satellite Attitude Control in the Presence of Inertia and CMG Actuator Uncertainties," *IEEE American Control Conference*, 2008.

[6] Lichter, M. D. and Dubowsky, S., "Estimation of State, Shape, and Inertial Parameters of State Objects from Sequence of Range Images," *SPIE Intelligent Robotics and Computer Vision*, 2003.

[7] Linares, R., Jah, M., Crassidis, J., Leve, F., Demars, J., and Kelecy, T., "Astrometric and Photometric Data Fusion for Inactive Space Object Feature Estimation," *IAF Inernational Astronautical Congress*, 2011.

[8] Shuster, M. D., "A Survey of Attitude Representations," *Journal of the Astronautical Sciences*, Vol. 41, No. 4, Oct.-Dec. 1993, pp. 439–517.

[9] Borderies, N. and Longaretti, P., "A New Treatment of the Albedo Radiation Pressure in the Case of a Uniform Albedo and of a Spherical Satellite," *Celestial Mechanics and Dynamical Astronomy*, Vol. 49, No. 1, March 1990, pp. 69–98.

[10] Vallado, D. A., *Fundamentals of Astrodynamics and Applications*, McGraw-Hill, New York, NY, $3^{rd}$ ed., 1997.

[11] Ashikmin, M. and Shirley, P., "An Anisotropic Phong Light Reflection Model," Tech. Rep. UUCS-00-014, University of Utah, Salt Lake City, UT, 2000.

[12] Julier, S. J., Uhlmann, J. K., and Durrant-Whyte, H. F., "A New Method for the Nonlinear Transformation of Means and Covariances in Filters and Estimators," *IEEE Transactions on Automatic Control*, Vol. AC-45, No. 3, March 2000, pp. 477–482.

[13] Crassidis, J. L. and Markley, F. L., "Unscented Filtering for Spacecraft Attitude Estimation," *Journal of Guidance, Control and Dynamics*, Vol. 26, No. 4, July-Aug. 2003, pp. 536–542.

[14] Jah, M. and Madler, R., "Satellite Characterization: Angles and Light Curve Data Fusion for Spacecraft State and Parameter Estimation," *Proceedings of the Advanced Maui Optical and Space Surveillance Technologies Conference*, Vol. 49, Wailea, Maui, HI, Sept. 2007, Paper E49.

[15] Wetterer, C. J. and Jah, M., "Attitude Estimation from Light Curves," *Journal of Guidance, Control and Dynamics*, Vol. 32, No. 5, Sept.-Oct. 2009, pp. 16482.

[16] Schaub, H. and Junkins, J. L., "Stereographic Orientation Parameters for Attitude Dynamics: A Generalization of the Rodrigues Parameters," *Journal of the Astronautical Sciences*, Vol. 44, No. 1, Jan.-March 1996, pp. 1–20.